The Mechanism of UV-A Radiation-Induced Inhibition of Photosystem II Electron Transport Studied by EPR and Chlorophyll Fluorescence†

Imre Vass,*,‡ Enikö Turcsányi,‡ Elefterios Touloupakis,§ Demetrios Ghanotakis,§ and Vasili Petrouleas||

Institute of Plant Biology, Biological Research Center, Szeged, Hungary, Department of Chemistry, University of Iraklion, Crete, Greece, and Institute of Materials Science, National Center for Scientific Research "Demokritos", Attikis, Greece

Received April 9, 2002; Revised Manuscript Received June 6, 2002

ABSTRACT: The UV-A (320−400 nm) component of sunlight is a significant damaging factor of plant photosynthesis, which targets the photosystem II complex. Here we performed a detailed characterization of UV-A-induced damage in photosystem II membrane particles using EPR spectroscopy and chlorophyll fluorescence measurements. UV-A irradiation results in the rapid inhibition of oxygen evolution accompanied by the loss of the multiline EPR signal from the S_2 state of the water-oxidizing complex. Gradual decrease of EPR signals arising from the $Q_A^-Fe^{2+}$ acceptor complex, Tyr-D°, and the ferricyanide-induced oxidation of the non-heme Fe^{2+} to Fe^{3+} is also observed, but at a significantly slower rate than the inhibition of oxygen evolution and of the multiline signal. The amplitude of Signal II_{fast}, arising from Tyr-Z° in the absence of fast electron donation from the Mn cluster, was gradually increased during the course of UV-A treatment. However, the amount of functional Tyr-Z decreased to a similar extent as Tyr-D as shown by the loss of amplitude of Signal II_{fast} that could be measured in the UV-A-treated particles after Tris washing. UV-A irradiation also affects the relaxation of flash-induced variable chlorophyll fluorescence. The amplitudes of the fast (600 μs) and slow (2 s) decaying components, assigned to reoxidation of Q_A^- by Q_B and by recombination of $(Q_AQ_B)^-$ with donor side components, respectively, decrease in favor of the 15−20 ms component, which reflects PQ binding to the Q_B site. In the presence of DCMU, the fluorescence relaxation is dominated by a 1 s component due to recombination of Q_A^- with the S_2 state. After UV-A radiation, this is partially replaced by a much faster component (30−70 ms) arising from recombination of Q_A^- with a stabilized intermediate PSII donor, most likely Tyr-Z°. It is concluded that the primary damage site of UV-A irradiation is the catalytic manganese cluster of the water-oxidizing complex, where electron transfer to Tyr-Z° and P_{680}^+ becomes inhibited. Modification and/or inactivation of the redox-active tyrosines and the Q_AFe^{2+} acceptor complex are subsequent events. This damaging mechanism is very similar to that induced by the shorter wavelength UV-B (280−320) radiation, but different from that induced by the longer wavelength photosynthetically active light (400−700 nm).

Light is a well-known damaging factor of the photosynthetic apparatus both in the visible and in the ultraviolet spectral range. Due to the recent depletion of the stratospheric ozone layer, which selectively absorbs the harmful UV-B radiation (280−320 nm), a special emphasis has been devoted to studying the mechanism and potential consequences of UV-B damage in photosynthetic organisms (*1*, *2*). However, the intensity of the UV-A (320−400 nm) spectral range is at least 10 times higher in natural sunlight than that of UV-B, and its penetration to the Earth is not attenuated significantly by the ozone layer or other components of the atmosphere (*3*). Studies performed in intact and isolated systems indicate that the most detrimental component of natural sunlight is the UV-A radiation in regard to damaging photosynthesis (*3*−*5*).

Despite its importance concerning inhibition of photosynthesis, our knowledge is far more limited about the effects of UV-A as compared to visible and UV-B light. The data available on UV-A indicate that this spectral range inhibits photosynthetic growth (*6*, *7*), accelerates leaf senescense (*8*), and impairs photosynthetic electron transport around PSII[1] (*7*). In a recent study, we have shown that the primary target of UV-A in the photosynthetic apparatus is the photosystem II (PSII) complex (*5*).

PSII is a water/plastoquinone oxido/reductase embedded in the thylakoid membrane, which transfers the electrons liberated from light-induced oxidation of water to membrane-soluble plastoquinone molecules [for a review, see (*9*)]. The redox cofactors of PSII electron transport are bound to or

† This work was supported by grants from the Hungarian Granting Agency, OTKA (D 29107, T 030592), INCO-Copernicus (ERB IC15-CT98-0126), NATO [outreach (LG 940992) 5408], and Greek−Hungarian bilateral cooperation (TET Gr-6/99).

* To whom correspondence should be addressed. Tel/Fax: 36-62-433-434. E-mail: imre@everx.szbk.u-szeged.hu.

‡ Biological Research Center.

§ University of Iraklion.

|| National Center for Scientific Research "Demokritos".

[1] Abbreviations: PSII, photosystem II; P_{680}, reaction center chlorophyll of PSII; Q_A, first quinone electron acceptor of PSII; Q_B, second quinone electron acceptor of PSII; cyt *b*-559, cytochrome *b*-559; Pheo, pheophytin electron acceptor of PSII; Tyr-Z, immediate tyrosine electron donor of P_{680}; Tyr-D, accessory tyrosine electron donor of P_{680}.

10.1021/bi020272+ CCC: $22.00
Published on Web 07/19/2002

contained by the D1 and D2 protein subunits which form the reaction center of PSII (*10, 11*). Water oxidation is catalyzed by a cluster of four Mn ions, and electrons liberated during this process are transferred to the reaction center chlorophyll, P680, via a redox-active tyrosine residue, called Tyr-Z, of the D1 protein. PSII contains another redox-active tyrosine, called Tyr-D located on the D2 subunit, which can donate electrons to P680, but not connected to the water-oxidizing complex. On the acceptor side of PSII, the electron produced by the light-induced charge separation event reduces a pheophytin molecule and then the first, Q_A, and second, Q_B, plastoquinone (PQ) electron acceptors [see ref (*9*)]. Q_A is a firmly bound component of the reaction center complex which undergoes one-electron reduction. In contrast, Q_B is a mobile electron carrier which takes up two electrons sequentially from Q_A before leaving its binding site formed by the D1 protein.

The harmful effects of UV-A radiation on PSII function are manifested as inhibition of electron transport (*7, 8*), a modified pattern of flash-induced oxygen evolution, and modified Q_B binding affinity (*5*). In addition, UV-A induces the degradation of the D1 and D2 reaction center proteins (*5*). However, the mechanistic details of these effects have not been clarified.

In the present work, we performed a thorough, comparative characterization of the UV-A effect on the main putative targets in PSII using low-temperature EPR spectroscopy in combination with chlorophyll fluorescence measurements and protein analysis. Our results demonstrate that the primary lesion occurs in the Mn cluster of water oxidation, with subsequent impairment of the quinone electron acceptors and the redox-active tyrosines.

MATERIALS AND METHODS

Sample Preparation. PSII particles were isolated from spinach as described earlier (*12*) and were stored at −80 °C until use in 0.4 M sucrose, 5 mM $MgCl_2$, 10 mM NaCl, and 40 mM Mes (pH 6.5) at 2−3 mg of Chl mL^{-1}.

UV-A Treatment. UV-A irradiation was performed in open, cylindrical glass containers in which the PSII membranes of 200 μg of Chl mL^{-1} concentration formed a layer of 10 mm height, with continuous stirring at room temperature. A Vilbert-Lourmat VL-215A lamp was used as UV-A light source, with maximal emission at 365 nm, and about 40 nm bandwidth. To screen out any UV-B or UV-C contribution from the lamp, a plastic filter was applied, which cut all radiation below 320 nm. The UV-A intensity was 13.8 W/m^{-2} as measured by a Cole-Parmer radiometer (97503-00) equipped with a 365 nm sensor, which corresponds to about 47 $\mu E\ m^{-2}\ s^{-1}$.

Variable Chlorophyll Fluorescence Measurements. Steady-state variable fluorescence was measured by a PAM machine (WALZ, Effeltrich, Germany) using a Q_A-Data (Turku, Finland) computer-controlled data acquisition system.

Fluorescence Relaxation Kinetics. Flash-induced increase and subsequent decay of chlorophyll fluorescence yield was measured by a double-modulation fluorometer (P. S. I. Instruments, Brno) (*13*), in the 150 μs−100 s time range as described earlier (*14*). Analysis of the fluorescence relaxation kinetics was based on the widely used model of the two-electron gate (*15*−*17*). According to this model, the fast (few hundred microseconds) decay component reflects Q_A^- reoxidation via forward electron transport in centers which contain bound PQ at the Q_B site. The middle (few milliseconds) phase arises from Q_A^- reoxidation in centers which had an empty Q_B site at the time of the flash and have to bind a PQ molecule from the PQ pool. Finally, the slow (few seconds) phase reflects Q_A^- reoxidation via back-reaction with the S_2 state of the water-oxidizing complex via the $Q_A^-Q_B \leftrightarrow Q_AQ_B^-$ equilibrium. Since the fluorescence yield is not linearly correlated with the amount of Q_A^-, the relative Q_A^- concentration was estimated according to the model of Joliot (*18*) using 0.5 for the value of the energy-transfer parameter between PSII units. Multicomponent deconvolution of the relaxation curves was performed by using a fitting function with two exponential and one hyperbolic components:

$$F_{v,corr} = A1*\exp(-t/\tau 1) + A2*\exp(-t/\tau 2) + A3/(1 + t/\tau 3)$$

Here, $F_{v,corr}$ is the variable fluorescence yield corrected for nonlinearity. $A1$, $A2$, and $A3$ are the amplitudes. $\tau 1$, $\tau 2$, and $\tau 3$ are the time constants from which the half-lifetimes can be calculated as $t_{1/2} = \ln 2*\tau$ for the exponential components, and $t_{1/2} = \tau$ for the hyperbolic component. The two exponential components are used to describe the fast and middle phases, whereas the hyperbolic component is used for describing the slow phase (*14*).

Oxygen Evolution Measurements. Steady-state rates of oxygen evolution were measured using a Hansatech DW2 O_2 electrode at a light intensity of 1000 $\mu E\ m^{-2}\ s^{-1}$ in the presence of 0.5 mM 2,5-dimethyl-*p*-benzoquinone as electron acceptor. Typically, 2 mL of cells at 10 μg of Chl *a* mL^{-1} was used in each measurement.

EPR Measurements. X-band low-temperature EPR spectra were recorded at 9.42 GHz microwave frequency with a Bruker ESP 200D spectrometer equipped with an Oxford Instruments cryostat and temperature controller. Illumination of the EPR samples was performed in an unsilvered Dewar from an 860 W projector lamp through a heat-absorbing $CuSO_4$ filter at 77 K (in liquid nitrogen) or at 200 K (in acetone cooled by liquid nitrogen). Data acquisition and analysis were performed by homemade software. The kinetic EPR measurements were carried out with a Bruker ER 200D X-band spectrometer in a flat sample cell at 1 mg of Chl/mL as described earlier (*19*). The saturation exciting flashes were provided by an EG&G Xenon flash lamp system. The rise and decay of the photoinduced signal was followed by a DSP model 2824SA transient recorder/signal analyzer.

Protein Analysis. D1 protein degradation was followed by SDS−PAGE on a 12−17% linear acrylamide gradient gel containing 6 M urea, as described previously (*12*). For immunoblotting, the resolved proteins were transferred to a nitrocellulose filter (Sartorius 45 μm) by electroblotting and were identified by using polyclonal antibody raised against the C-terminal part of D1 protein (kind gift Dr. Peter Nixon, Imperial College, London). The reaction was visualized by a colorimetric method, and the immunodecorated blots were analyzed by an Eagle Eye gel documentation system.

RESULTS

UV-A Effects on the Donor Side of PSII. A likely target of UV-A radiation in PSII is the water-oxidizing complex

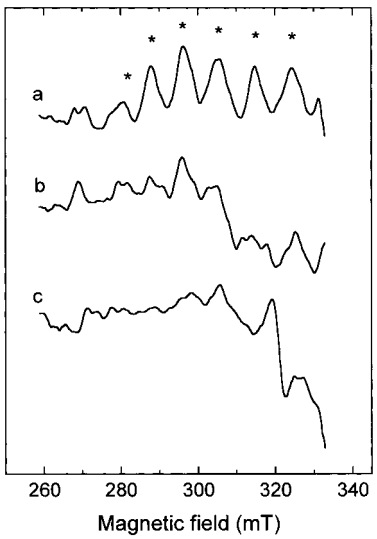

FIGURE 1: Effect of UV-A radiation on the multiline EPR signal of PSII membrane particles. The multiline signal was induced by 10 min illumination at 200 K in samples which had been exposed to UV-A irradiation for 0 (a), 60 (b), and 180 min (c). The six-line EPR signal from free manganese was eliminated by addition of 3 mM EDTA. The spectra are shown as light minus dark difference spectra. EPR conditions: temperature = 10 K, microwave power = 20 mW, modulation amplitude = 2.5 mT.

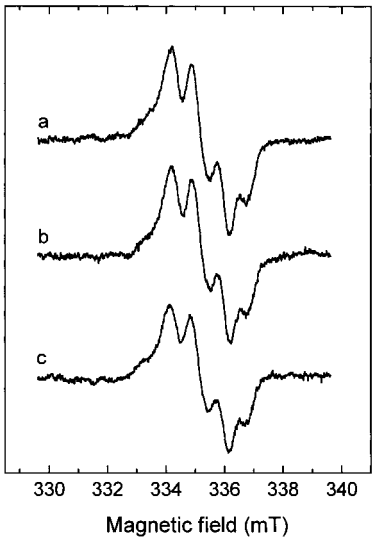

FIGURE 2: Effect of UV-A radiation on Signal II_{slow} of PSII membrane particles. The dark-stable Signal II_{slow} was measured in samples which had been irradiated with UV-A for 0 (a), 120 (b), and 180 min (c). Before the EPR measurements, all samples were illuminated with visible light for 1 min to oxidize Tyr-D uniformly. EPR conditions: temperature = 10 K, microwave power = 200 nW, modulation amplitude = 0.32 mT.

(*5*, *7*). We applied EPR spectroscopy to clarify the site and extent of its damage by UV-A irradiation.

(A) The S_2-State Multiline Signal. Redox functioning of the water-oxidizing complex can be directly monitored by measuring the so-called multiline EPR signal from the S_2 state (*20*). The size of the multiline signal was strongly decreased after 60 min UV-A irradiation, and was almost completely abolished after 180 min (Figure 1). In our experiments, the multiline signal was induced by illumination at 200 K. At this temperature, the S_1 to S_2 transition takes place, and the electron can be transferred to Q_A, but the Q_A to Q_B transition is inhibited. Thus, limited multiline signal formation in the UV-A-irradiated PSII membranes reports a lesion of electron transport between the water-oxidizing complex and Q_A. The S_2 state of the Mn cluster gives rise to another EPR signal at $g = 4.1$ [for a review, see (*21*)]. During the course of UV-A irradiation, the $g = 4.1$ signal decreased to a similar extent as the multiline signal (not shown). This observation excludes the possibility that the loss of the multiline signal could be due to its conversion into the $g = 4.1$ signal and provides further support for UV-A-induced impairment of electron extraction from the Mn cluster.

(B) Signal II_{slow}. Tyrosines absorb in the ultraviolet region with peaks at around 280 nm in their neutral form, and at around 300 nm in their oxidized radical form, as demonstrated for Tyr-Z (*22*−*24*). Based on these absorption characteristics, both Tyr-Z and Tyr-D are considered as being targets of UV-B radiation (*12*, *25*). However, the absorption spectrum extends also to the UV-A range and thus tyrosines could be prone to UV-A damage, too. To follow UV-A-induced changes in the redox function of Tyr-D, we measured the EPR signals arising from the oxidized radical form of this residue. Tyr-D° is remarkably stable in the dark and gives rise to the EPR Signal II_{slow} (*26*). As a consequence of UV-A irradiation, the amplitude of Signal II_{slow} gradually decreases with increasing irradiation time. However, its loss is less pronounced than that of the multiline signal, and about 80% of the original Signal II_{slow} can still be detected after 180 min irradiation (Figure 2). This observation implies not only that Tyr-D or its environment is damaged by UV-A, but also that Tyr-D is clearly more resistant against the UV-A attack than the water-oxidizing complex.

(C) Signal II_{fast}. In functional PSII centers, oxidized Tyr-Z is rapidly rereduced by the Mn cluster. Therefore, the EPR signal, called Signal $II_{very\ fast}$, arising from Tyr-Z can only be observed with time-resolved measurements in the microsecond range (*27*). When electron transport from the Mn cluster is inhibited, the lifetime of Tyr-Z° increases to hundreds of milliseconds and the so-called Signal II_{fast} appears (*28*). To monitor the effect of UV-A radiation on the transient formation of Signal II_{fast}, we applied time-resolved EPR measurements. In the nonirradiated sample, Signal II_{fast} is almost completely absent. The small residual signal can be attributed to PSII centers in which the Mn cluster was damaged during isolation (Figure 3). However, after inactivation of the water-oxidizing complex by Tris washing, the full Signal II_{fast} can be observed. During the course of UV-A irradiation, Signal II_{fast} gradually appears without Tris washing, but the full amplitude of the signal, which is observed after Tris washing, decreases. These observations are consistent with the inhibition of electron donation from the Mn cluster to Tyr-Z° and also with the partial impairment of Tyr-Z functioning.

UV-A Effects on the Quinone−*Iron Acceptor Complex.* The series of one-electron-transfer steps within the PSII complex is interfaced to the two-electron reduction of plastoquinone by the so-called two-electron gate consisting of Q_A and Q_B in close interaction with the non-heme iron [for reviews, see (*15*, *29*, *30*)]. Due to their absorption in the UV-B spectral range, the quinone electron acceptors are frequently considered as important targets of UV-B radiation in PSII (*31*−*34*). Since plastosemiquinones also have an

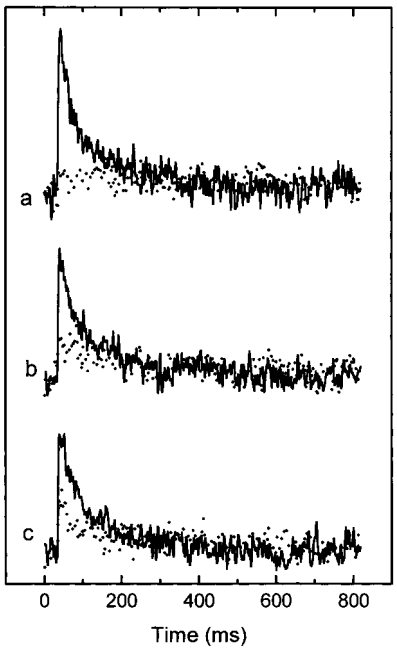

FIGURE 3: Effect of UV-A radiation on the flash-induced formation of Signal II_{fast}. The kinetic traces were measured at the low-field peak position of Signal II in nonirradiated controls (a) and after 60 (b) and 180 (c) min of UV-A irradiation. The dotted traces were measured without further treatment, whereas the solid curves were obtained after Tris washing of the samples. The PSII membranes contained an equimolar (3 mM) mixture of ferricyanide and ferrocyanide as an acceptor system. Each curve is the average of 200 traces measured with 0.3 Hz repetition rate. EPR conditions: temperature = 293 K, microwave power = 20 mW, modulation amplitude = 0.4 mT, time constant = 1 ms.

absorption band at around 360−380 nm, they may be potential UV-A targets, too. To study the extent of UV-A-induced damage to the function of the quinone−iron acceptor complex, we applied EPR and chlorophyll fluorescence measurements.

(A) The $Q_A^-Fe^{2+}$ Signal. The interaction of Q_A^- and Fe^{2+} gives rise to an EPR signal in the $g = 1.8-1.9$ range, providing a useful marker of Q_A reduction (*35*−*37*). To avoid limitation of electron transfer from the water-oxidizing complex, Q_A reduction was induced by illumination at 77 K. At this temperature, the primary charge separation and electron transfer from Tyr-Z to Q_A is active, but the $S_1 \rightarrow S_2$ transition is inhibited and alternative donors, such as cyt *b*-559, the accessory chlorophylls, and carotenoids, can provide the electron for Q_A reduction. The measurements in Figure 4 show that the $Q_A^-Fe^{2+}$ signal is suppressed in the UV-A-irradiated PSII membranes. It is also clear that the inhibition of the $Q_A^-Fe^{2+}$ signal is less pronounced than that observed for the multiline signal, since after 180 min irradiation about 60% of the original $Q_A^-Fe^{2+}$ signal can still be induced (Figure 4) in contrast to the almost complete loss of the multiline signal (Figure 1). To clarify if the loss of the $Q_A^-Fe^{2+}$ signal is due to direct UV-A damage of the quinone−iron complex or of the alternative donors which function at 77 K, Q_A reduction was also induced chemically by dithionite. The effect of UV-A radiation on the size of the dithionite-induced $Q_A^-Fe^{2+}$ signal was similar to that observed after 77 K illumination (not shown). This observation shows that the loss of the $Q_A^-Fe^{2+}$ signal is not due to the impairment of the alternative PSII donors, but is the consequence of UV-A irradiation on the Q_A quinone−iron complex.

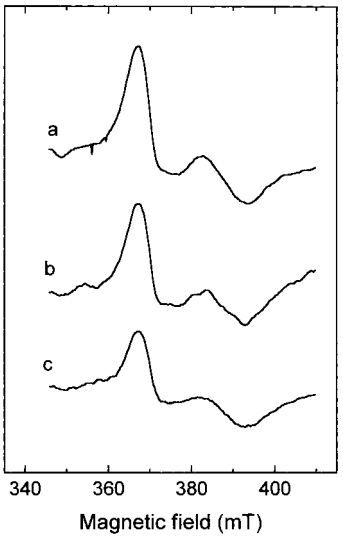

FIGURE 4: Effect of UV-A radiation on the $Q_A^-Fe^{2+}$ EPR signal of PSII membrane particles. The reduction of Q_A was induced by 10 min illumination at 77 K in samples which had been exposed to UV-A irradiation for 0 (a), 60 (b), and 180 min (c) and contained 3 mM EDTA to remove free manganese. Sodium formate (100 mM) was added after the UV-A treatment to enhance the $Q_A^-Fe^{2+}$ signal (*49*). The curves shown are light minus dark difference spectra. EPR conditions: temperature = 4.2 K, microwave power = 32 mW, modulation amplitude = 3.2 mT.

(B) The Fe^{3+} Signal. Since the $Q_A^-Fe^{2+}$ signal arises from the interaction of Q_A^- and Fe^{2+} (*35*, *36*), its decrease upon UV-A irradiation can be induced by damage either of $Q_A(^-)$ or of the iron. This uncertainty can be clarified by verifying directly the presence and redox activity of the non-heme iron by measuring the EPR signal from its oxidized (Fe^{3+}) state. In our experiments, the iron was oxidized in the dark by potassium ferricyanide, and the oxidized minus reduced EPR spectra were obtained in the control and irradiated samples (Figure 5). The Fe^{3+} signal in the nonirradiated control is characterized by peaks at around $g = 8$ and 5.6 (*38*). UV-A irradiation resulted in the gradual loss of the $g = 8$ and 5.6 peaks. The extent by which the $g = 8$ and 5.6 signals of Fe^{3+} are decreased is similar or even smaller than the decrease of the $Q_A^-Fe^{2+}$ signal; i.e., 70% of the original Fe^{3+} remains after 180 min irradiation (Figure 5, see also Figure 9 below). This observation implies that prolonged UV-A exposure affects the redox function of the Fe, but at the same time excludes the possibility that a preferential effect on the iron would be responsible for the UV-A-induced loss of the $Q_A^-Fe^{2+}$ signal.

UV-A Effects on the Reoxidation of Q_A^-. The functions of both quinone components of the quinone−iron acceptor complex, Q_A and Q_B, can be studied by measuring flash-induced changes in the yield of chlorophyll fluorescence. The reduction of Q_A upon flash excitation results in a prompt increase of chlorophyll fluorescence yield, that is followed by a dark decay in the hundred microseconds to tens of seconds time range due to reoxidation of Q_A^- by various pathways.

In the nonirradiated control particles, the relaxation is characterized by a fast (≈600 μs), a middle (≈18 ms), and

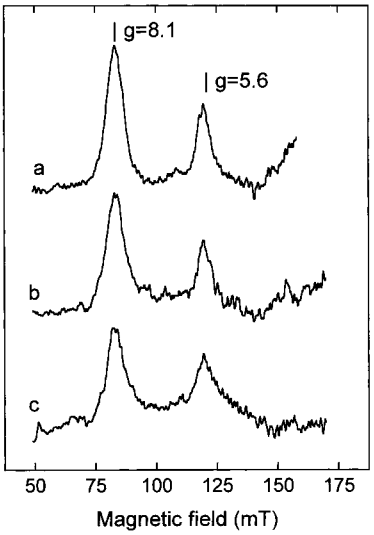

FIGURE 5: Effect of UV-A radiation on the Fe^{3+} EPR signal of PSII membrane particles. The oxidation of the non-heme iron from its Fe^{2+} to the Fe^{3+} form was induced by incubating the samples in the presence of 5 mM potassium ferricyanide for 30 min in the dark at room temperature. The samples had previously been irradiated with UV-A for 0 (a), 60 (b), and 180 min (c). The curves shown are the oxidized minus reduced difference spectra obtained after and before the incubation with FeCy, respectively. EPR conditions: temperature = 4.2 K, microwave power = 8 mW, modulation amplitude = 1.6 mT.

a slow (≈2 s) phase. As a result of UV-A irradiation, the initial amplitude of the fluorescence signal decreased, but the overall decay kinetics were only slightly affected (Figure 6). The relative amplitudes of the fast and slow phases decreased from 39 to 34% and from 35 to 30%, respectively, whereas the relative amplitude of the middle phase increased from 27 to 37% (Table 1). However, the time constants remained practically unchanged.

In the presence of DCMU, which blocks the reoxidation of Q_A^- by forward electron transfer, the fluorescence relaxation reflects the reoxidation of Q_A^- via recombination with donor side components. In UV-A-irradiated samples, the initial amplitude decreased, and the decay kinetics were accelerated (Figure 7). Analysis of these decay curves showed that in the nonirradiated control a slow-decaying component, with about 1 s time constant, dominated the decay. As a result of UV-A irradiation, a fast component (4 ms) appeared whose relative amplitude increased to 16% after 180 min irradiation (Table 1). Besides this, a phase

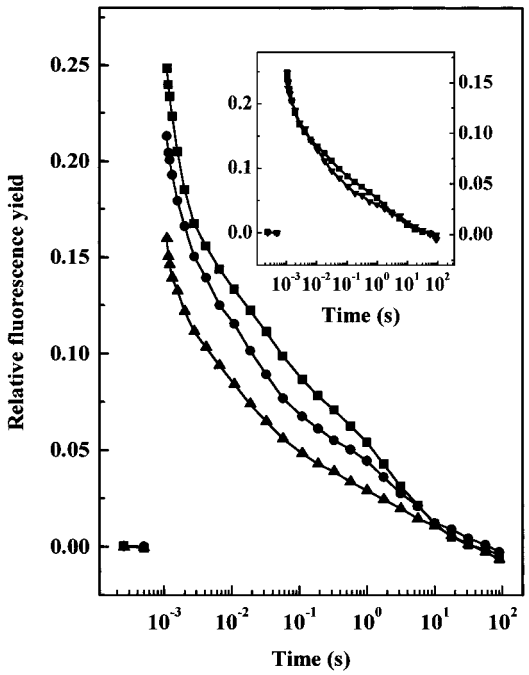

FIGURE 6: Effect of UV-A radiation on the flash-induced change of chlorophyll fluorescence yield. The kinetic traces were measured in PSII particles exposed to 0 (squares), 60 (circles), and 180 min (triangles) UV-A irradiation. The flash was fired at the 10^{-3} s time point and the first measurement taken 150 μs after the flash. The inset shows the 0 min (squares) and 180 min (triangles) traces normalized to the same initial amplitude.

with 30−70 ms time constant was induced. Its relative amplitude reached 10% after 180 min irradiation. In parallel with these changes, the relative amplitude of the 1 s phase decreased to 74%.

Effect of UV-A on the D1 Protein. UV-A damages both the D1 and D2 reaction center subunits of PSII with a more pronounced effect on D1 than D2 (*5*). However, there was no information available on the site where the protein cleavage occurs. Here we used an antibody targeted against the C-terminal part of the D1 protein to identify the UV-A-induced breakdown products of D1. As shown in Figure 8, the main fragment was a 20 kDa C-terminal product, with a smaller amount of a 25 kDa fragment. As our comparative experiment shows, these fragments are of the same size as the well-characterized breakdown products induced by UV-B radiation (*39*).

Table 1: Decay Kinetics of Flash-Induced Variable Fluorescence[a]

duration of UV-A irradiation (min)	total amplitude (%)	fast phase τ (ms) [amp (%)]	middle phase τ (ms) [amp (%)]	slow phase τ (s) [amp (%)]
		No Addition		
0	100[b]	0.59 ± 0.03 (38.9 ± 3)[c]	18.4 ± 1.3 (26.6 ± 2)	1.5 ± 1.5 (34.5 ± 1)
60	84.3 ± 2	0.68 ± 0.03 (34.9 ± 3)	17.5 ± 3.5 (34.3 ± 2)	2.1 ± 1.2 (30.8 ± 1)
180	62.5 ± 2	0.60 ± 0.04 (33.6 ± 3)	17.5 ± 2.0 (36.7 ± 3)	1.9 ± 2.0 (29.7 ± 2)
		With DCMU		
0	100	− (0)	− (0)	1.04 ± 1 (100)
60	88.6 ± 2	4.4 ± 0.8 (6.8 ± 0.8)	28.8 ± 1.3 (4.7 ± 1)	1.05 ± 0.1 (88.8 ± 2)
180	67 ± 2	4.4 ± 0.6 (15.6 ± 0.6)	69.5 ± 1.3 (10.2 ± 2)	1.32 ± 0.3 (74.2 ± 1)

[a] PSII particles were irradiated with UV-A for the indicated periods, and relaxation of flash-induced fluorescence yield was measured without addition or in the presence of 10 μM DCMU as in Figures 6 and 7. [b] Values represent the amplitude of the total variable fluorescence in percent of that in the nonirradiated control. [c] Values in parentheses are relative amplitudes in percent of total variable fluorescence obtained after the given UV-A irradiation time. Standard errors of the calculated parameters are also indicated.

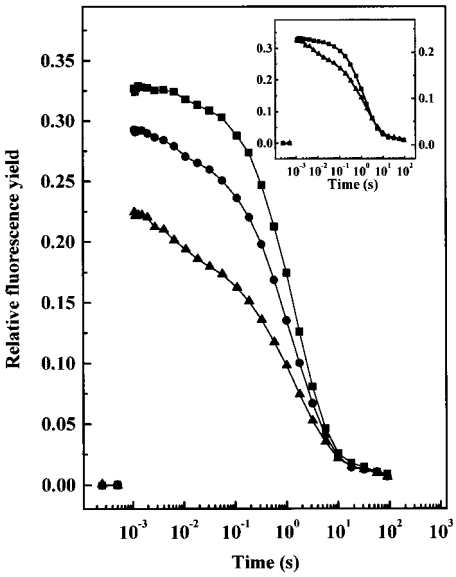

FIGURE 7: Effect of UV-A irradiation on the relaxation of flash-induced chlorophyll fluorescence yield in the presence of DCMU. The measurements were performed in PSII particles, which were exposed to UV-A irradiation for 0 (squares), 60 (circles), and 180 min (triangles). Before measurements, the samples were treated with 10 μM DCMU. The inset shows the 0 (squares) and 180 min curves (triangles) normalized to the same initial amplitude.

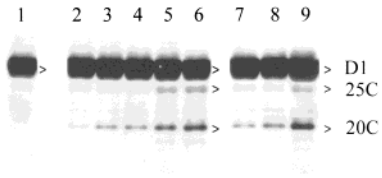

FIGURE 8: UV-A radiation-induced fragmentation of the D1 protein. PSII membranes were irradiated with UV-A for 0 (lane 1), 15 (lane 2), 40 (lane 3), 60 (lane 4), 120 (lane 5), and 180 min (lane 6). The full-length D1 protein and its degradation products were detected by polyclonal antibody directed against the C-terminal of D1. For comparison, the fragmentation pattern induced by UV-B irradiation is shown by lanes 7 (30 min UV-B), 8 (60 min UV-B), and 9 (120 min UV-B).

DISCUSSION

UV-A radiation has been shown to damage the photosystem II complex (*5*, *7*). Previous studies have indicated the water-oxidizing complex and the Q_AQ_B two-electron gate as putative molecular targets of UV-A within PSII (*5*). However, the importance and relative sensitivity of these target sites in the overall UV-A effect were not clarified.

UV-A Effects on the Water-Oxidizing Complex. The inhibitory courses of the studied PSII activity parameters are compared in Figure 9. Inhibition of steady-state oxygen evolution, that reflects the loss of electron transport through PSII, is followed closely by the decline of the S_2-state multiline signal, and the alternative $g = 4.1$ signal (not shown). Charge stabilization in the S_2 state requires noniterrupted electron transport from the water-oxidizing complex to Q_A. The significantly smaller loss of the $Q_A^-Fe^{2+}$ signal as compared to the S_2-state multiline signal shows that damage of Q_A or of electron transport from P_{680} to Q_A cannot be the primary cause for the inhibition of S_2-state formation. Instead, the limited multiline signal formation should be due to damage of the catalytic manganese cluster.

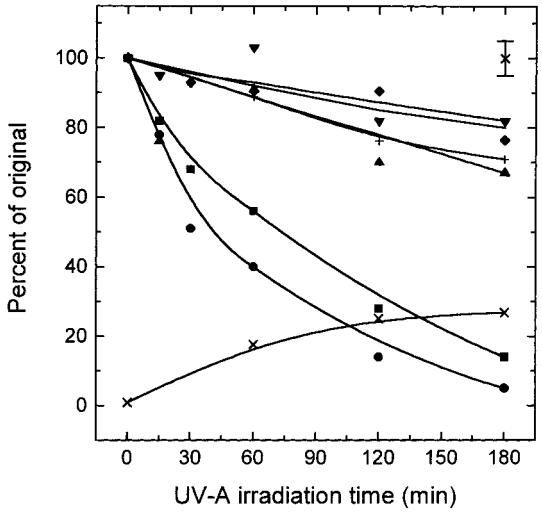

FIGURE 9: Time course of PSII activity loss during UV-A irradiation. The EPR signals, oxygen evolution, and variable fluorescence were measured as described under Materials and Methods as well as in Figures 1−5. The data were replotted as a function of UV-A irradiation time as a percentage of their value in the nonirradiated controls: steady-state oxygen evolution (filled circles), S_2-state multiline signal (squares), Signal II_{slow} (downward triangles), the $g = 8.06$ peak of the Fe^{3+} signal (diamonds), the $Q_A^-Fe^{2+}$ signal induced by illumination at 77 K (upward triangles), Signal II_{fast} measured before (tilted crosses) and after Tris treatment (standing crosses). The typical error of the measurements is indicated by the error bar.

Electron donation from the water-oxidizing complex to P_{680} is mediated by Tyr-Z. Tyrosines absorb at around 280 nm in the neutral form and at around 300 nm in the oxidized radical form, which extends into the UV-A region. The decline of Signal II_{slow} and of Signal II_{fast} in Tris-treated samples shows that both Tyr-D and Tyr-Z are indeed damaged by UV-A. However, this effect is much smaller than the loss of oxygen evolution and of the multiline signal (Figure 9). Consequently, the redox-active tyrosines can also be excluded from the primary targets of UV-A radiation.

The crucial observation concerning the site where the first step of UV-A induced damage occurs in PSII is the induction of Signal II_{fast} without Tris treatment, and the appearance of fast fluorescence decay in the presence of DCMU (Figures 3 and 7, Table 1). The induction of Signal II_{fast} in about 30% of PSII centers after 180 min UV-A treatment demonstrates the inability of the Mn cluster to donate electrons to Tyr-Z°. To ensure that the acceptor side of PSII does not get blocked during the repetitive flashes, the samples contained a mixture of ferrocyanide and ferricyanide as artificial acceptor. Therefore, the relaxation kinetics (≈100 ms) are determined by slow electron donation to Tyr-Z° from exogenous donors without being influenced by recombination with acceptor side components. The appearance of fast decaying fluorescence component(s) in the presence of DCMU demonstrates that the S_2 state has been replaced by much less stable donor(s) in the recombination reaction of Q_A^- (*14*). The fast decaying fluorescence was resolved into two phases with 4 and 30−70 ms time constants. The 4 ms phase is considerably slower than the $P_{680}^+Q_A^-$ recombination, which occurs around 100 μs in Mn-depleted PSII particles (*40*), but much faster than the Tyr-Z°Q_A^- recombination (see below). This phase may originate from the reoxidation of Q_A^- with an intermediate donor component,

whose reoxidation by the Mn cluster is impaired by UV-A. Possible candidates for this donor are Chl_Z^+, Car^+, or P_{680}^+. The time constant of the slower components is similar to that assigned to Tyr-Z°Q_A^- recombination in cyanobacterial mutants [20−50 ms, (*41*)], and dark-grown *Chlamydomonas* that lack the functional Mn cluster [90 ms, (*42*)], or in isolated BBY particles in which the Mn cluster was inactivated by NH_2OH treatment [36 ms, (*43*)]. Based on these data, we propose that the 30−70 ms phase reflects the recombination of Q_A^- with Tyr-Z° in centers where the Mn cluster is inactivated by UV-A radiation. The gradual increase of the time constant from 30 to 70 ms with the progress of UV-A treatment indicates the stabilization of the Tyr-Z°Q_A^- charge pair due to a UV-A-induced modification of the Tyr-Z°/Tyr-Z and/or the Q_A/Q_A^- redox potentials.

The fast fluorescence decay occurs in about 25% of the centers as compared to about 30% of PSII in which Signal II_{fast} is formed. Direct kinetic comparison between the relaxation of fluorescence and Signal II_{fast} is hampered by the different experimental conditions, i.e., the presence of DCMU during the fluorescence measurements and of the ferrocyanide−ferrocyanide acceptor system in the EPR samples. However, the similar fraction of centers in which fast fluorescence and Signal II_{fast} is observed without Tris treatment supports the idea that fast fluorescence decay in the presence of DCMU arises from the donor side inhibited centers.

UV-A Effects on the $Q_AFe^{2+}Q_B$ Acceptor Complex. The plastoquinone electron acceptors of PSII absorb in the UV-C and UV-B range, with the main peaks at 250 and 310 nm in the oxidized and the semireduced state, respectively, and show only weak absorption in UV-A. We observed that the light-induced EPR signal arising from the interaction of Q_A^- and Fe^{2+} is decreased as a consequence of UV-A irradiation (Figure 5). However, as discussed above, the loss of the $Q_A^-Fe^{2+}$ signal occurs much slower than the inhibition of oxygen evolution and of the multiline signal (Figure 9), which exclude Q_A as being the main target of UV-A action in PSII. The decrease of the light-induced $Q_A^-Fe^{2+}$ EPR signal may not necessarily reflect damage of Q_A itself. Inhibition of electron transfer from the PSII donor side to Q_A, modification or damage of the non-heme iron, and also alteration of the protein environment around the Q_A site could lead to the absence of the $Q_A^-Fe^{2+}$ signal.

The first alternative can be ruled out by showing that chemical reduction of Q_A by dithionite is inhibited in the irradiated samples to the same extent as the light-induced reduction of Q_A. Thus, despite the early inhibition of the water-oxidizing complex, electron transport from the donor side of PSII is not limiting Q_A reduction during 77 K illumination. The functioning donors for this process could be Tyr-Z, cyt *b*-559, Chl_z, or carotene.

The second alternative concerns the modification or loss of the non-heme iron. In the UV-A-irradiated samples, spontaneous iron oxidation has not been observed (not shown). In addition, the amount of ferricyanide-oxidizable Fe^{2+} decreased to a somewhat lesser extent than the $Q_A^-Fe^{2+}$ signal (Figure 9). Thus, the loss of the $Q_A^-Fe^{2+}$ signal cannot be initiated by the preferential modification or release of the non-heme iron. However, the decrease of the Fe^{3+} signal indicates that the number of centers in which the non-heme iron is located in the undisturbed protein environment is decreasing.

The electrons from Q_A are accepted by the second quinone, Q_B, whose function may also be affected by UV-A radiation. This question was approached by measuring the decay kinetics of the flash-induced fluorescence yield, which reflects the reoxidation of Q_A^- (Figure 6). The dominating fast kinetics of the fluorescence decay (in the 600 μs and 18 ms time range) represent electron transfer from Q_A^- to Q_B, whereas the slow kinetics (in the few seconds time range) represent the recombination of Q_A^-, via the $Q_A^-Q_B \leftrightarrow Q_AQ_B^-$ equilibrium, with the positively charged S states of the water-oxidizing complex (*15*, *29*). The decreased initial amplitude of the flash-induced fluorescence signal in UV-A-irradiated samples is consistent with the decrease of functional PSII centers which can transfer electrons from the water-oxidizing complex to Q_A. The relative amplitudes of the fast and middle phases are expected to reflect the amount of PSII centers in which the Q_B site is occupied and vacant, respectively (*16*). Thus, the increased amplitude of the middle phase which is accompanied by the decrease of the fast and slow phases indicates that UV-A irradiation decreases the binding affinity of PQ at the Q_B site.

UV-A Effects on the Protein Structure of the PSII Reaction Center. UV-A-induced degradation of the D1 (and D2) reaction center proteins has been demonstrated earlier (*5*); however, the cleavage site was not identified. Here we show that UV-A radiation induces a 20 kDa C terminal fragment as the main breakdown product (Figure 8). This fragment has the same size as that induced by UV-B radiation, and most likely can be assigned to the same cleavage site, which was proposed to be located in the middle of the second transmembrane helix of D1 (*39*). Thus, it appears that UV-A and UV-B damage the D1 protein by the same or very similar mechanism. As summarized in Figure 9, the loss of $Q_A^-Fe^{2+}$, Fe^{3+} Signal II_{fast}, and Signal II_{slow} EPR signals show similar courses. This situation might indicate that the redox activities of the above components are lost due to a structural change of the PSII reaction center.

Mechanistic Aspects of the UV-A Effect in PSII. The mechanisms by which the PSII redox components are impaired by UV-A are very similar to those induced by UV-B. In the case of Q_A, Tyr-Z, and Tyr-D, a direct destruction of the molecules could occur. However, the possibility that the redox function of these components is impaired due to damage of their protein environment is also likely (see above).

Damage or alteration of the protein binding site of the catalytic Mn cluster is also the most likely scenario for the inactivation of the water-oxidizing function, since the Mn ions themselves are not modified by UV-A. Mn is expected to be ligated by histidines, aspartates, or glutamates [for a recent review, see (*44*)] which are less UV-sensitive than the aromatic tyrosine, phenylalanine, and tryptophan as well as cysteine (*45*). Thus, UV-A-induced alteration of the protein environment around the manganese cluster may occur in more indirect ways than direct hit of Mn-ligating amino acid residues.

Comparison of the action spectra of UV-induced inhibitory effects with the absorbance of the putative target molecules is often useful to identify the species that mediate the UV damage. The most detailed action spectrum of light-induced

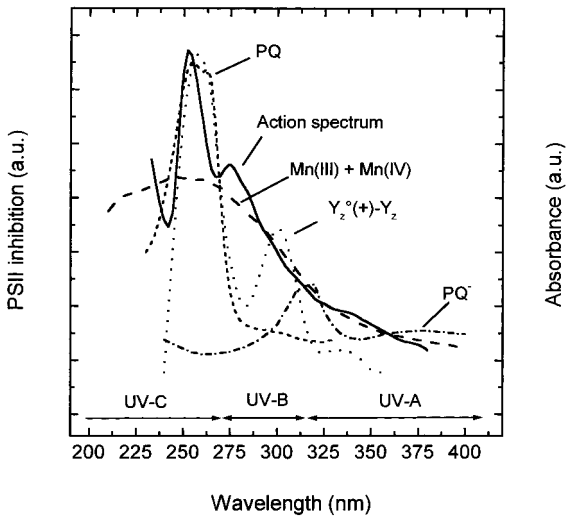

FIGURE 10: Action spectrum of UV-induced inactivation of PSII in comparison with the absorption spectrum of potential UV targets. The action spectrum of PSII inactivation measured by Jones and Kok (*46*) (solid line) is compared to the absorption spectrum of Tyr-Z°−Tyr-Z (*22*) (dotted line), the absorption spectrum of Mn-(III) and Mn(IV) gluconate (*49*) (dashed line), and the absorption spectrum of plastoquinone in the oxidized (short-dashed line) and in the semireduced form (dash−dotted line) (*50*).

PSII damage comes from the work of Jones and Kok (*46*), who measured the inhibition of Hill activity, i.e., electron transport through PSII (Figure 10). Obviously, the match between the action spectrum, which peaks at 250 nm, and the absorbance of single molecular targets is satisfactory only for limited spectral ranges (Figure 10). In the 280−400 nm range, there is a remarkable similarity between the action spectrum and the absorption of Mn(III) and Mn(IV) ions, which constitute the catalytic site of the water-oxidizing complex in its higher oxidation states. Above 330 nm, the absorbance of plastosemiquinone also gives a good match. Thus, absorption by the Mn cluster is likely to be a main sensitizer in the whole UV-A and UV-B range, whereas oxidized tyrosines may have an additional role in the UV-C range. On the other hand, semireduced plastoquinone could be responsible for sensitizing the alteration of the Q_B site.

It also important to note that the mechanism of UV-A-induced damage is clearly different from that induced by the longer wavelength photosynthetically active radiation (400−700 nm). Photoinhibition by visible light has its main action site at the level of the Q_A and Q_B acceptors and does not damage the water-oxidizing complex [see (*47*, *48*)]. However, photodamage by visible light is enhanced if water oxidation is inactivated by other factors [see (*48*)]. Thus, impairment of the water-oxidizing complex by UV-A could accelerate the photoinhibitory effect of the visible spectral range of natural sunlight.

Concluding Remarks. Our results show that UV-A radiation has multiple action sites in isolated PSII preparations. The water-oxidizing complex appears to be most sensitive. The Q_AFe complex and the redox-active tyrosines as well as the Q_B binding site are also affected by UV-A, but to a smaller extent than the water-oxidizing complex. This situation is very similar to that observed after inhibition by UV-B, although the damaging efficiency of UV-A is smaller. These findings, in agreement with the identical cleavage site of the D1 protein, point to the basically same damaging mechanism of UV-A and UV-B, mediated by senzitizers which have smaller absorbance in UV-A as compared to UV-B. Since the intensity of the UV-A spectral range is at least 10 times higher than that of UV-B in the natural sunlight, UV-A should be considered as a significant damaging factor of plant photosynthesis under natural conditions.

ACKNOWLEDGMENT

We appreciate the help of Dr. Cornelia Spetea with the D1 protein immunoblot experiments and Dr. Ch. Goussias with the low-temperature EPR measurements.

REFERENCES

1. Smith, R. C., Prézelin, B. B., Baker, K. S., Bidigare, R. R., Boucher, N. P., Coley, T., Karentz, D., MacIntyre, S., Matlick, H. A., Menzies, D., Ondrusek, M., Wan, Z., and Waters, K. J. (1995) *Science 255*, 952−959.
2. Campbell, D., Erikson, M.-J., Öquist, G., Gustafsson, P., and Clarke, A. K. (1998) *Proc. Natl. Acad. Sci. U.S.A. 95*, 364−369.
3. Holm-Hansen, O., Lubin, D., and Helbling, E. W. (1993) in *Environmental UV Photobiology* (Young, A. R., Björn, L. O., Moan, J., and Nultsch, W., Eds.) pp 379−426, Plenum Press, New York and London.
4. Cullen, J. J., Neale, P., and Lesser, M. P. (1992) *Science 258*, 646−650.
5. Turcsányi, E., and Vass, I. (2000) *Photochem. Photobiol. 72*, 513−520.
6. Klein, M. R., Edsall, C. P., and Gentile, C. A. (1965) *Plant Physiol. 40*, 903−906.
7. Hirosawa, T., and Miyachi, S. (1982) *Plant Sci. Lett 28*, 291−298.
8. Joshi, P. N., Biswal, B., Kulandaivelu, G., and Biswal, U. C. (1994) *Radiat. Environ. Biophys. 33*, 167−176.
9. Andersson, B., and Styring, S. (1991) *Curr. Top. Bioenerg. 16*, 1−81.
10. Nanba, O., and Satoh, K. (1987) *Proc. Natl. Acad. Sci. U.S.A. 84*, 109−112.
11. Zouni, A., Witt, H. T., Kern, J., Fromme, P., Kraus, N., Saenger, W., and Orth, P. (2001) *Nature 409*, 739−743.
12. Vass, I., Sass, L., Spetea, C., Bakou, A., Ghanotakis, D., and Petrouleas, V. (1996) *Biochemistry 35*, 8964−8973.
13. Trtilek, M., Kramer, D. M., and Koblizek, M. (1997) *J. Lumin. 72*−*74*, 597−599.
14. Vass, I., Kirilovsky, D., and Etienne, A.-L. (1999) *Biochemistry 38*, 12786−12794.
15. Diner, B. A. (1998) in *Photosynthesis: Molecular Biology of Energy Capture* (McIntosh, L., Ed.) pp 337−360, Academic Press, San Diego.
16. Crofts, A., Baroli, I., Kramer, D. M., and Taoka, S. (1993) *Z. Naturforsch. 48C*, 259−266.
17. Renger, G., Eckert, H.-J., Bergmann, A., Bernarding, J., Liu, B., Napiwotzki, A., Reifarth, F., and Eichler, H.-J. (1995) *Aust. J. Plant Physiol. 22*, 167−181.
18. Joliot, A., and Joliot, P. (1964) *C. R. Acad. Sci. 258*, 4622−4625.
19. Bakou, A., and Ghanotakis, D. F. (1993) *Biochim. Biophys. Acta 1141*, 303−308.
20. Dismukes, G. C., and Siderer, Y. (1981) *Proc. Natl. Acad. Sci. U.S.A. 78*, 274−278.
21. Miller, A.-F., and Brudvig, G. W. (1991) *Biochim. Biophys. Acta 1056*, 1−18.
22. Dekker, J. P., van Gorkom, H. J., Brok, M., and Ouwehand, L. (1984) *Biochim. Biophys. Acta 764*, 301−309.
23. Gerken, S., Brettel, K., Schlodder, E., and Witt, H. T. (1988) *FEBS Lett. 237*, 69−75.
24. Diner, B. A., and de Vitry, C. (1995) in *Advances in Photosynthesis Research* (Sybesma, C., Ed.) Vol. 1, pp 407−411, Martinus Nijhoff/Dr. W. Junk, The Hague, The Netherlands.
25. Yerkes, C. T., Kramer, D. M., Fenton, J. M., and Crofts, A. R. (1990) in *Current Research in Photosynthesis* (Baltscheffsky, M., Ed.) Vol. II, pp II.6.381−II.6.384, Kluwer Academic Publishers, Dordrecht, The Netherlands.
26. Babcock, G. T., and Sauer, K. (1973) *Biochim. Biophys. Acta 325*, 483−503.

27. Hoganson, C. W., and Babcock, G. T. (1988) *Biochemistry 27*, 5848−5855.
28. Blankenship, R. E., Babcock, G. T., Warden, J. T., and Sauer, K. (1975) *FEBS Lett. 51*, 287−293.
29. Crofts, A. R., and Wraight, C. A. (1983) *Biochim. Biophys. Acta 726*, 149−185.
30. Diner, B. A., Petrouleas, V., and Wendolski, J. J. (1991) *Physiol. Plant. 81*, 423−436.
31. Greenberg, B. M., Gaba, V., Canaani, O., Malkin, S., Mattoo, A. K., and Edelman, M. (1989) *Proc. Natl. Acad. Sci. U.S.A. 86*, 6617−6620.
32. Trebst, A., and Depka, B. (1990) *Z. Naturforsch. 45C*, 765−771.
33. Melis, A., Nemson, J. A., and Harrison, M. A. (1992) *Biochim. Biophys. Acta 1100*, 312−320.
34. Jansen, M. A. K., Gaba, V., and Greenberg, B. M. (1998) *Trends Plant Sci. 3*, 131−135.
35. Nugent, J. H. A., Diner, B. A., and Evans, M. C. W. (1981) *FEBS Lett. 124*, 241−244.
36. Rutherford, A. W., and Zimmermann, J.-L. (1984) *Biochim. Biophys. Acta 767*, 168−175.
37. Vermaas, A. F. J., and Rutherford, A. W. (1984) *FEBS Lett. 175*, 243−248.
38. Petrouleas, V., and Diner, B. A. (1986) *Biochim. Biophys. Acta 849*, 264−275.
39. Friso, G., Spetea, C., Giacometti, G. M., Vass, I., and Barbato, R. (1993) *Biochim. Biophys. Acta 1184*, 78−84.
40. Conjeaud, H., and Mathis, P. (1986) *Biophys. J. 49*, 1215−1221.
41. Chu, H.-A., Nguyen, A. P., and Debus, R. J. (1994) *Biochemistry 33*, 6137−6149.
42. Rova, M., Mamedov, F., Magnuson, A., Fredrikkson, P.-O., and Styring, S. (1998) *Biochemistry 37*, 11039−11045.
43. Buser, C. A., Thompson, L. K., Diner, B. A., and Brudvig, G. W. (1990) *Biochemistry 29*, 8977−8985.
44. Diner, B. A. (2001) *Biochim. Biophys. Acta 1503*, 147−163.
45. Vladimirov, Y. A., Roshchupkin, D. I., and Fesenko, E. E. (1970) *Photochem. Photobiol. 11*, 227−246.
46. Jones, L. W., and Kok, B. (1966) *Plant Physiol. 41*, 1037−1043.
47. Vass, I., Styring, S., Hundal, T., Koivuniemi, A., Aro, E.-M., and Andersson, B. (1992) *Proc. Natl. Acad. Sci. U.S.A. 89*, 1408−1412.
48. Aro, E.-M., Virgin, I., and Andersson, B. (1993) *Biochim. Biophys. Acta 1143*, 113−134.
49. Bodini, M. E., Willis, L. A., Riechel, T. L., and Sawyer, D. T. (1976) *Inorg. Chem. 15*, 1538−1543.
50. Amesz, J. (1977) in *Encyclopedia of Plant Physiology* (Trebst, A., and Avron, M., Eds.) Vol. 5, pp 238−246, Springer-Verlag, Berlin.

BI020272+